**Neuron, Volume *109***

## Supplemental Information

# Non-canonical glutamate signaling in a genetic model of migraine with aura

**Patrick D. Parker, Pratyush Suryavanshi, Marcello Melone, Punam A. Sawant-Pokam, Katelyn M. Reinhart, Dan Kaufmann, Jeremy J. Theriot, Arianna Pugliese, Fiorenzo Conti, C. William Shuttleworth, Daniela Pietrobon, and K.C. Brennan**

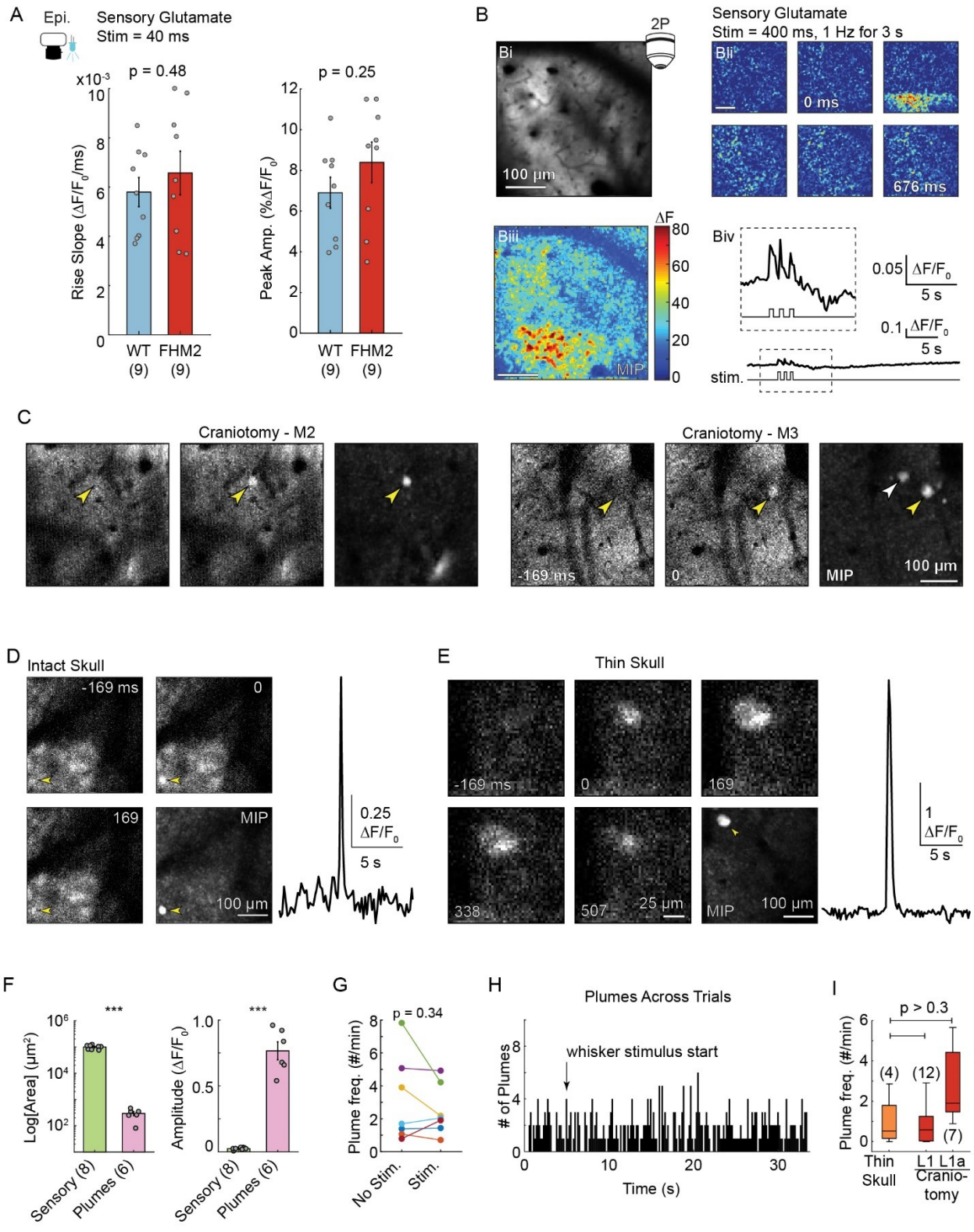
A
Epi.
Sensory Glutamate
Stim = 40 ms
p = 0.48
x10-3
Rise Slope (ΔF/F0/ms)
WT (9)
FHM2 (9)
p = 0.25
Peak Amp. (%ΔF/F0)
WT (9)
FHM2 (9)
B
2P
Bi
100 µm
Sensory Glutamate
Stim = 400 ms, 1 Hz for 3 s
Bii
0 ms
676 ms
Biii
ΔF
MIP
Biv
0.05 ΔF/F0
5 s
0.1 ΔF/F0
5 s
stim.
C
Craniotomy - M2
Craniotomy - M3
-169 ms
0
MIP
100 µm
D
Intact Skull
-169 ms
0
169
MIP
100 µm
0.25 ΔF/F0
5 s
E
Thin Skull
-169 ms
0
169
338
507
25 µm
MIP
100 µm
1 ΔF/F0
5 s
F
***
Log[Area] (µm2)
Sensory (8)
Plumes (6)
***
Amplitude (ΔF/F0)
Sensory (8)
Plumes (6)
G
p = 0.34
Plume freq. (#/min)
No Stim.
Stim.
H
Plumes Across Trials
whisker stimulus start
# of Plumes
Time (s)
I
p > 0.3
Plume freq. (#/min)
(4)
(12)
(7)
Thin Skull
L1 L1a Cranio-tomy

**Figure S1. Examples of glutamate signaling *in vivo* (related to Figures 1 – 2).**

(**A**) Following a 40 ms whisker stimulation, the slope of the rise (left) and the peak amplitude (Amp.; right) of the fluorescent glutamate response was similar in WT and FHM2 mice. Glutamate fluorescence was measured with epifluorescence (Epi.) in the same mice and recordings as Figure 1. Two-sample t-test.

(**B**) Glutamate response to whisker stimulation using two-photon (2P) from a single trial. (Bi) Average intensity projection (AIP) of iGluSnFR fluorescence. (Bii) Panels show the glutamate response over time (change in fluorescence; ΔF) during whisker stimulation (0 ms; 169 ms between panels). Notice the band of increased fluorescence restricted to the bottom of the panel immediately after whisker stimulation, followed by a low amplitude increase in fluorescence across the FOV in subsequent panels. This artifact is due to the raster scanning of the 2P microscope and temporal under-sampling of the glutamate response (Fs = 5.92 Hz). This artifact was never seen with the faster sampling rate and the use of a camera with epifluorescence. Panels depict the glutamate response to the first stimulus of a train of stimulations (400 ms, 1 Hz for 3 s). (Biii) Maximum intensity projection (MIP) of the entire stimulus train shows a spatially broad increase in glutamate across the FOV with 2P (384 $\mu m^2$), as well as more localized puncta within the response area. (Biv) Quantification of the glutamate response with magnification (inset). Scale of the bottom trace is similar to 2P recordings in Figure 2 for comparing whisker mediated response amplitude to glutamatergic plume amplitude.

(**C**) Examples of individual plumes (yellow arrowheads) across time in unprocessed frames, as well as MIP from bandpass filtered ΔF image series (see STAR Methods). M2 and M3 are examples from two mice using a craniotomy and implanted glass coverslip.

The white arrowhead in the MIP of M3 indicates a second plume that occurred during the trial but is not shown in the individual frames to the left.

(**D – E**) Examples of plumes with an intact skull (no thinning; n = 1 mouse) (D) and a thin skull (a thin portion of bone left over the brain; representative of n= 4 mice) (E) that were recorded to determine whether plumes were due to removal of the skull. Quantification of fluorescence intensity to the right. See panel I for quantification of plume frequency with thin skull.

(**F**) Area (left) and amplitude (right) of plumes vs whisker induced glutamate responses using 2P recordings (*** = $p < 1*10^{-7}$; two-sample t-test). FHM2 mice.

(**G**) Plume frequency did not differ between trials with and without whisker stimulation (paired-sample t-test; n = 7 FHM2 mice).

(**H**) Frequency histogram of when plumes occurred during whisker stimulation trials (n = 338 plumes from 6 FHM2 mice). Note that plumes do not cluster in time around the start of whisker stimulation.

(**I**) Given the high frequency of plumes in L1a near the surface of the brain, we performed thin skull experiments to determine whether plumes were caused by removing the skull during craniotomy. The thin skull preparation decreased the resolution during imaging, making it difficult to distinguish between L1a and L1b. Thus, the frequency of plumes during thin skull was compared to L1a and L1 as a whole (L1a and L1b combined) from craniotomy experiments (Wilcoxon rank-sum). While the craniotomy may have potentially increased the frequency of plumes in L1a (though the difference was insignificant), all 4 mice with thin skull preparation showed plumes. All FHM2 mice.

F, H omitted one mouse due to slower sampling frequency (2.96 Hz). All figures from FHM2 mice, except where indicated as WT in A.

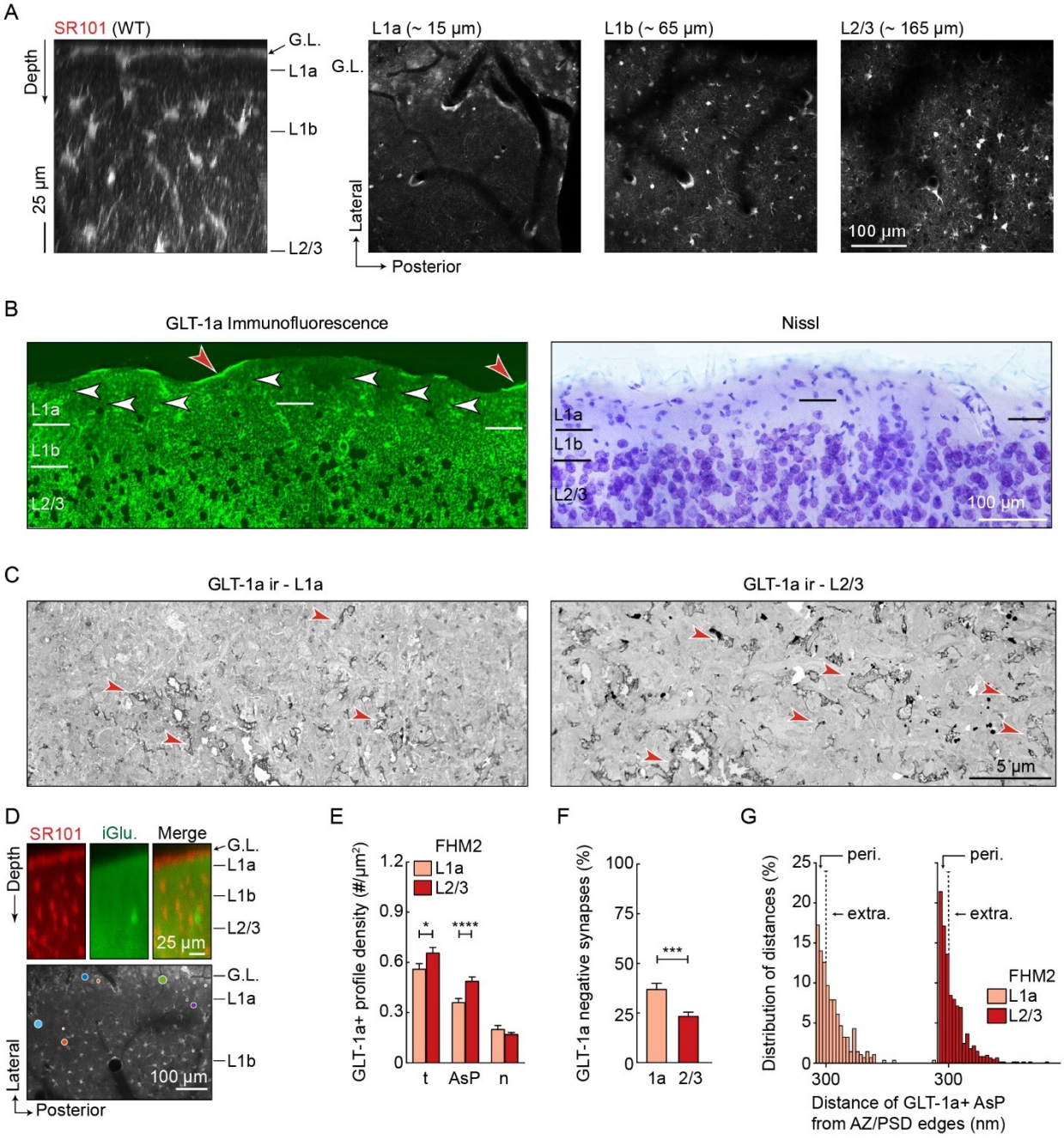
A
SR101 (WT)
Depth
25 μm
G.L.
L1a
L1b
L2/3
L1a (~ 15 μm)
L1b (~ 65 μm)
L2/3 (~ 165 μm)
Lateral
Posterior
100 μm
B
GLT-1a Immunofluorescence
Nissl
L1a
L1b
L2/3
100 μm
C
GLT-1a ir - L1a
GLT-1a ir - L2/3
5 μm
D
SR101
iGlu.
Merge
Depth
Lateral
Posterior
25 μm
100 μm
E
FHM2
L1a
L2/3
GLT-1a+ profile density (#/μm²)
t
AsP
n
F
GLT-1a negative synapses (%)
1a
2/3
G
Distribution of distances (%)
peri.
extra.
FHM2
Distance of GLT-1a+ AsP from AZ/PSD edges (nm)

**Figure S2. L1a anatomy (related to Figure 3).**

(**A**) SR101 revealed a decreased incidence of astrocyte somas below the glia limitans (G.L.) in L1a *in vivo*. Example z-stack along the cortical depth (left; MIP of 33.4 μm along the medial/lateral axis) and corresponding images (right) from a single WT mouse illustrate the laminar density of astrocytes in L1a through L2/3.

(**B**) Left: low magnification of confocal microscopical fields reveals several irregular areas of reduced GLT-1a immunofluorescence (ir) within L1a (white arrowheads). This is an expanded version of the same section in Figure 3C. Right: Representative Nissl staining of a section of the same series used for GLT-1a immunofluorescence. Red arrowheads indicate putative GLT-1a immunopositive (+) glia limitans.

(**C**) Low magnified electron microscopic fields of immunoperoxidase pre-embedded material from WT mice exhibit a different frequency of GLT-1a immunopositive (+) profiles (characterized by dark electrodense products) in L1a (left) and L2/3 (right). Red arrowheads point to some examples of GLT-1a+ profiles.

(**D**) In a FHM2 mouse, iGluSnFR (iGlu.) and SR101 were combined to show the location of plumes relative to the band of decreased astrocyte somas below the glia limitans, within putative L1a. Top: Z-stack images recorded along the cortical depth *in vivo* from above the glia limitans (G.L.) down to ~ 180 μm (within L2/3). Images are a MIP of 57 μm along the medial/lateral axis. Bottom: Functional recordings revealed that plumes primarily occurred in L1a within or near the band of decreased astrocyte somas. AIP of 20 s recording with colored overlays to illustrate the location and size of plumes from a 10 min recording. Image was cropped and only SR101 is shown for clarity.

(**E – G**) Similar to Figure 3E – G, though for FHM2 mice.

(**E**) The density of GLT-1a+ astrocyte processes (AsP) was reduced in L1a compared to L2/3, resulting in a reduced total (t) density of GLT-1a+ profiles. n = neuronal. (Mann Whitney test).

(**F**) L1a contained a larger proportion of synapses with no GLT-1a immunoreactivity (GLT-1a negative) vs L2/3 (Mann Whitney test).

(**G**) For synapses containing an adjacent GLT-1a+ AsP, L1a contained a lower proportion of perisynaptic AsP [peri.; distance < 300 nm from the edge of the active zone (AZ)/post-synaptic density (PSD)] and greater proportion of extrasynaptic AsP (extra; distance > 300 nm) compared to L2/3 ($p = 0.025$; Fisher's test).

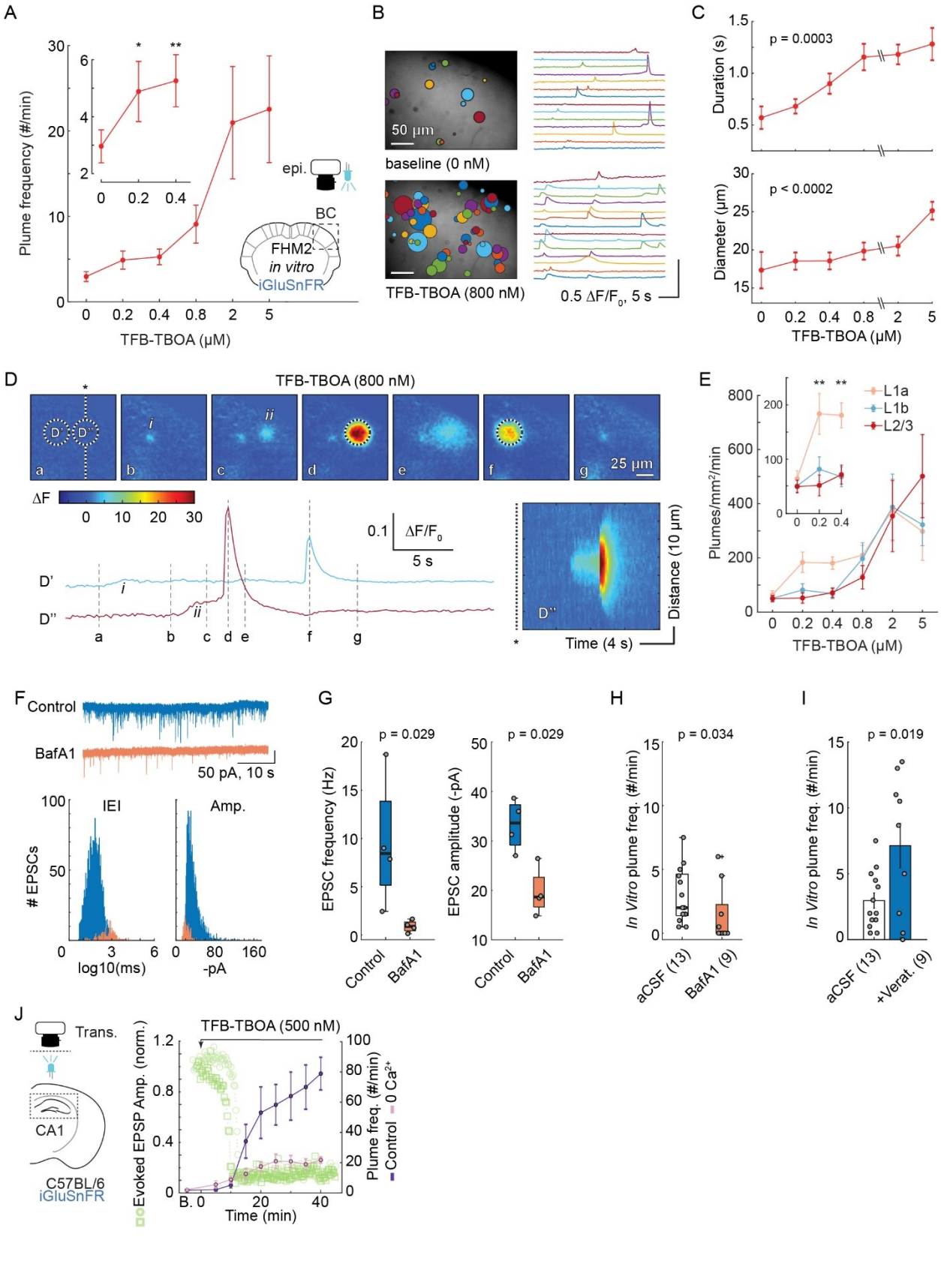
A
Plume frequency (#/min)
TFB-TBOA (µM)
epi.
BC
FHM2
in vitro
iGluSnFR
B
50 µm
baseline (0 nM)
TFB-TBOA (800 nM)
0.5 ΔF/F0, 5 s
C
p = 0.0003
Duration (s)
p < 0.0002
Diameter (µm)
TFB-TBOA (µM)
D
TFB-TBOA (800 nM)
25 µm
ΔF
0.1 ΔF/F0
5 s
D'
D''
Distance (10 µm)
Time (4 s)
E
L1a
L1b
L2/3
Plumes/mm²/min
TFB-TBOA (µM)
F
Control
BafA1
50 pA, 10 s
IEI
Amp.
# EPSCs
log10(ms)
-pA
G
p = 0.029
EPSC frequency (Hz)
p = 0.029
EPSC amplitude (-pA)
Control
BafA1
H
p = 0.034
In Vitro plume freq. (#/min)
aCSF (13)
BafA1 (9)
I
p = 0.019
In Vitro plume freq. (#/min)
aCSF (13)
+Verat. (9)
J
Trans.
CA1
C57BL/6
iGluSnFR
TFB-TBOA (500 nM)
Evoked EPSP Amp. (norm.)
Plume freq. (#/min)
Control
0 Ca2+
Time (min)

**Figure S3. Glutamate transporter function mediates plume characteristics, and bafilomycin A1 control experiments (related to Figures 3 and 4).**

(**A – E**) We found a dose-response of plume frequency, diameter and duration to increasing concentrations of TFB-TBOA in brain slices containing the barrel cortex (BC) from FHM2 mice (n = 13 slices from 4 mice), confirming the association of plume characteristics with glutamate clearance efficiency. Imaging performed with epiflorescence microscopy (Epi.).

(**A**) Plume frequency curve with increasing concentrations of the glutamate transporter inhibitor TFB-TBOA. Inset shows that plume frequency increased relative to baseline with sub-saturating concentrations of TFB-TBOA, 200 and 400 nM, within 5 and 10 min of the start of drug perfusion, respectively (repeated measures ANOVA with Dunnett's correction).

(**B**) AIP with plume overlays (left) and select plume traces (right) from a 2 min recording in the same brain slice with and without TFB-TBOA. Baseline = 0 nM.

(**C**) Effects of increasing TFB-TBOA concentration on plume duration and diameter (repeated measures ANOVA with Greenhouse-Geisser adjustment).

(**D**) With moderate to higher concentrations of TFB-TBOA (0.8 – 5 μM), plumes began to spatially and temporally overlap. In this example, smaller diameter and lower amplitude plumes (i and ii) arose and persisted prior to larger events originating from the same location (D' and D''). Images correspond with lower-case letters in traces below. Lower Right: a kymograph of D'' illustrates the spatial characteristics over time. Same slice as B.

(**E**) Distribution of plumes in supragranular layers in FHM2 brain slices. At baseline (TFB-TBOA = 0 μM), L1a had a slightly higher frequency of plumes relative to L1b and L2/3, though this was statistically insignificant ($p > 0.05$). TFB-TBOA potentiated the frequency of plumes in L1a compared to L1b and L2/3 at lower concentrations (0.2 and 0.4 μM; highlighted in inset), supporting our *in vivo* findings of an increased predisposition to plumes in L1a vs deeper layers (Figures 3 and S2). Higher concentration (0.8 – 5 μM) increased plumes to a similar frequency in all layers, suggesting TFB-TBOA overrode any laminar differences in clearance capabilities. This comparison was normalized for the size of a given layer within the field of view. Two-way repeated measure ANOVA with Bonferroni correction. Granular and subgranular layers were not measured.

(**F – I**) Bafilomycin A1 (BafA1) control experiments and additional comparisons.

(**F**) BafA1 control experiments measuring the inter-event interval (IEI) and amplitude (Amp.) of spontaneous excitatory postsynaptic currents (EPSC) using whole-cell patch-clamp (voltage clamp) of putative pyramidal neurons from L2/3 in WT cortical brain slices containing the barrel cortex. Top: Example traces from one neuron treated with BafA1 (+BafA1, 4 μM; +veratridine, 10 μM), and one control neuron (-BafA1; +veratridine). See STAR Methods for incubation protocol. Bottom: Distribution of IEI and Amp. for each group (n = 4 cells/group from 4 slices/group).

(**G**) Left: Slice averaged spontaneous EPSC frequency in Baf1A and control-treated L2/3 pyramidal neurons. Right: BafA1 also reduced the amplitude of the few remaining EPSCs. n = 4 cells/group from 4 slices/group.

(**H**) Plume frequency with Baf1A was decreased relative to slices in aCSF alone. aCSF slices = baseline (0 μM TFB-TBOA) from A of this figure. All slices from FHM2 mice.

(**I**) Control slices from our BafA1 experiments (-BafA1+Verat.) had an increased plume frequency compared to slices maintained in aCSF alone (two-sample t-test). aCSF slices = baseline (0 μM TFB-TBOA) from A of this figure. All slices from FHM2 mice. We confirmed this finding in FHM2 mice *in vivo* (Figures 4 and 5).

(**J**) Removing $Ca^{2+}$ from the bath inhibited the frequency of TFB-TBOA induced plumes in hippocampal slices from C57BL/6 mice [$p = 3.44*10^{-09}$ ($Ca^{2+}$), $2.26*10^{-08}$ (time), and $1.14*10^{-05}$ ($Ca^{2+}$ & time); repeated measures two-way ANOVA). In a subset of slices, we simultaneously measured evoked excitatory post-synaptic potentials (EPSP) using a field potential throughout the experiment. Long-term application of TFB-TBOA inhibited evoked EPSP amplitude in the hippocampus, indicative of suppressed action potentials (Tsukada et al., 2005), around the time of the steepest rise in plume frequency (light green; circles and squares indicate different brain slices; n = 2 slices). This data further supports our findings in FHM2 *in vivo* that plumes are dependent on $Ca^{2+}$ influx, though do not require action potentials (Figure 4). B. = baseline before drug application. Trans. = transillumination. Evoked EPSP amplitude was normalized (norm.) to pre-drug amplitudes (baseline).

A – E, H & I = slices from FHM2 mice. F & G, J = slices from WT mice. G & H = Wilcoxon rank-sum. * $p < 0.05$; ** $p < 0.01$

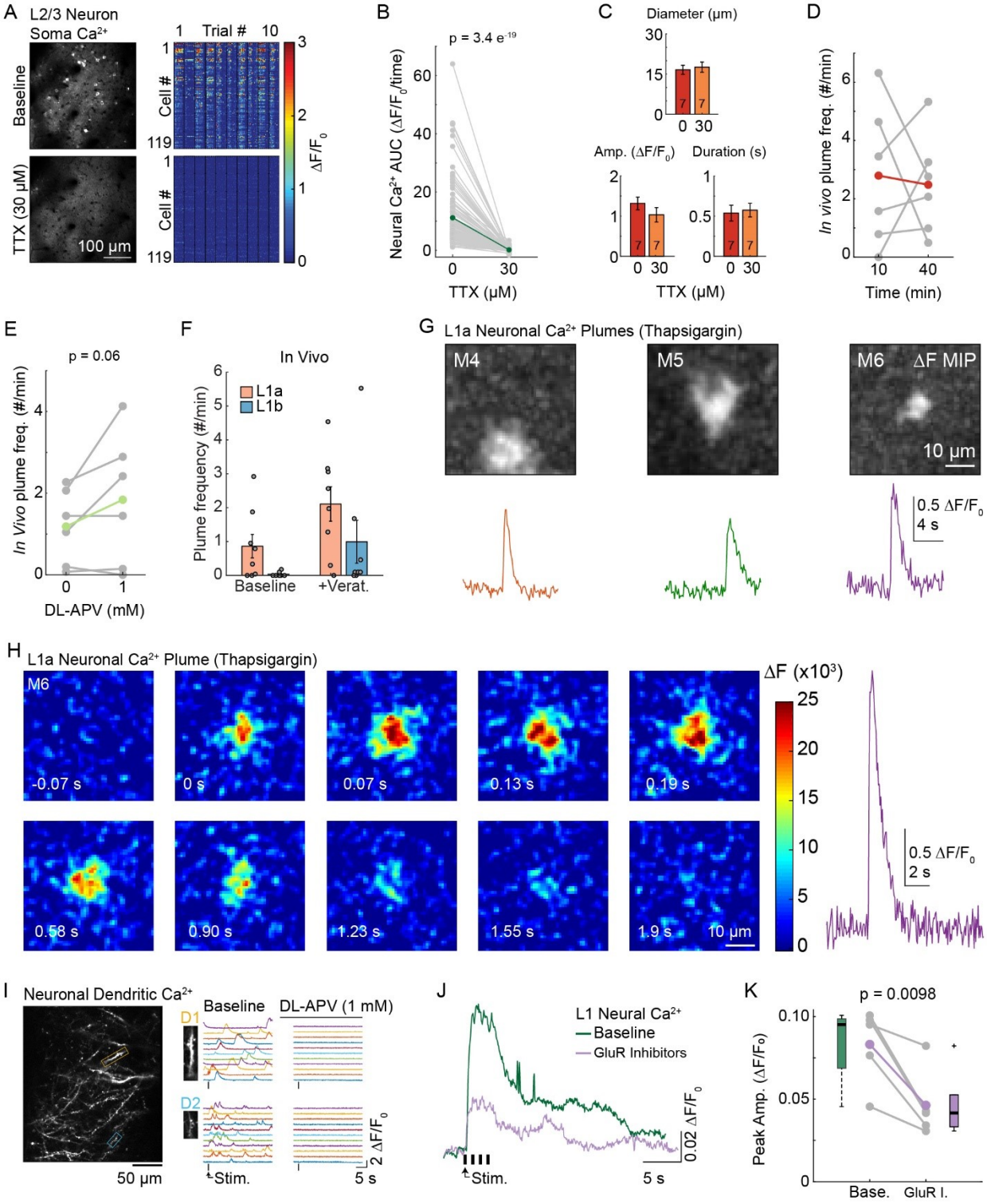
A
L2/3 Neuron
Soma Ca2+
Baseline
TTX (30 µM)
100 µm
Trial #
Cell #
ΔF/F0
B
p = 3.4 e-19
Neural Ca2+ AUC (ΔF/F0/time)
TTX (µM)
C
Diameter (µm)
Amp. (ΔF/F0)
Duration (s)
TTX (µM)
D
In vivo plume freq. (#/min)
Time (min)
E
p = 0.06
In Vivo plume freq. (#/min)
DL-APV (mM)
F
In Vivo
L1a
L1b
Plume frequency (#/min)
Baseline
+Verat.
G
L1a Neuronal Ca2+ Plumes (Thapsigargin)
M4
M5
M6
ΔF MIP
10 µm
0.5 ΔF/F0
4 s
H
L1a Neuronal Ca2+ Plume (Thapsigargin)
M6
-0.07 s
0 s
0.07 s
0.13 s
0.19 s
0.58 s
0.90 s
1.23 s
1.55 s
1.9 s
10 µm
ΔF (x10³)
0.5 ΔF/F0
2 s
I
Neuronal Dendritic Ca2+
Baseline
DL-APV (1 mM)
D1
D2
2 ΔF/F0
50 µm
Stim.
5 s
J
L1 Neural Ca2+
Baseline
GluR Inhibitors
0.02 ΔF/F0
Stim.
5 s
K
p = 0.0098
Peak Amp. (ΔF/F0)
Base.
GluR I.

**Figure S4: Control experiments for determining the source of glutamate during plumes (related to Figure 4).**

(**A – B**) The voltage-gated $Na^{2+}$ ($Na_V$) channel blocker tetrodotoxin (TTX) greatly inhibited neural $Ca^{2+}$ activity in L2/3 neural somas during whisker stimulation trials in Thy1-GCaMP6s mice (line GP4.3; Jackson Laboratory stock no: 024275) crossed with our FHM2 mice (*Atp1a2*$^{+/W887R}$). (A) AIP images (left) and intensity raster plots of $Ca^{2+}$ activity from 119 neural somas over 10 whisker stimulation trials (right) from the same animal before (baseline; top) and after 30 min superfusion of TTX (30 μM; bottom). (B) Quantification of the average $Ca^{2+}$ fluorescence for each neural soma across whisker stimulation trials demonstrates significant inhibition with TTX (n = 258 neurons from 3 mice). AUC = area under the curve. Note that $Ca^{2+}$ activity in neural somas measured with GCaMP6 is largely due to action potentials, with very little contribution from sub-threshold electrical activity, even *in vivo* (Chen et al., 2013), suggesting TTX sufficiently inhibited action potentials in our experiments.

(**C**) Plume characteristics during baseline vs TTX *in vivo*. Same mice as Figure 4B & C ($p > 0.05$ for all comparisons).

(**D**) The average change in plume frequency over time. In our TTX experiments, roughly half of the mice showed a decrease in plume frequency compared to baseline (4 out of 7 mice), while the other half showed either an increase or no change in plume occurrence with TTX (3 out of 7) (Figure 4C). To gain a better understanding of the variation in plume frequency over time in FHM2 mice, we performed a post hoc analysis comparing the frequency of plumes in mice with intact coverslips (no holes) and no experimental intervention. This analysis used the same time frame as our TTX and other pharmacology experiments, where the first 10 min of recording are equivalent to a ‘baseline’ and

recordings 30 – 40 min later represent a ‘drug’ condition. A third of the mice showed a large decrease in plume frequency over time (2 out of 6 mice), while the other mice showed either a large increase or relatively little change (4 out of 6 mice). However, the averaged frequency of the group remained stable over time, suggesting shifts in the group averaged plume frequency during pharmacology experiments are likely due to the experimental intervention. n = 6 FHM2 mice.

(**E**) The NMDA receptor blocker DL-APV did not inhibit the spontaneous plume frequency in FHM2 mice *in vivo*, suggesting plumes are not dependent on local presynaptic NMDA receptors. In fact, the group trended toward an increased average frequency, though this was insignificant. n = 5 FHM2 mice.

(**F**) Veratridine increased the frequency of plumes in both L1a and L1b in awake FHM2 mice. The frequency of plumes was higher in L1a compared to L1b at baseline (0 μM), confirming the increased incidence of plumes in L1a relative to deeper layers *in vivo* in a second set of FHM2 mice (see Figure 3B for initial characterization). Brief exposure to veratridine (+Verat.; 10 min, 100 – 150 μM, removed for recording) increased the frequency of plumes in both L1a and L1b relative to their baseline, indicating veratridine was able to induce plumes outside of L1a ($p = 0.045$ for layers and 0.025 for drug effects, two-way ANOVA; n = 8 mice). Even after veratridine exposer, the frequency of plumes was, on average, higher in L1a vs L1b. We did not record in L2/3 or deeper layers. Same mice as Figure 4F.

(**G – H**) Examples of plume-like neural $Ca^{2+}$ events (neural $Ca^{2+}$ plumes) observed in the neuropil of L1a with thapsigargin in FHM2.Thy1GCaMP6s mice (putative excitatory neurons). The neural $Ca^{2+}$ plumes depicted here were in different mice than those

described in Figure 4H – J (mouse #4 - #6 or M4 – M6). These events were recorded without glutamate receptor inhibitors, so they may comprise both pre- and postsynaptic neural $Ca^{2+}$ signaling. (G) The MIP from ΔF image stacks (top) with the corresponding trace of the normalized change in fluorescence for each neural $Ca^{2+}$ plume directly below (bottom). (H) Left: A panel of pseudocolored ΔF images depict a single neural $Ca^{2+}$ plume over time. Note the similarities in the spatial characteristic with glutamatergic plumes (Figures 2C, 7C, and S1C – E, as well as Movies S1 and S2), as the $Ca^{2+}$ plume starts from a central location and increases in size over time. Timestamps are relative to the start of the plume. Right: Quantification of the normalized change in fluorescence for the same $Ca^{2+}$ plume.

(**I – K**) Control experiments for glutamate receptor (GluR) inhibitors.

(**I**) Superfusion of the NMDA receptor inhibitor DL-APV (1 mM) inhibited neural dendritic $Ca^{2+}$ activity in awake mice. GCaMP6f was sparsely expressed in L2/3 neurons using a Cre-dependent viral injection method (see STAR Methods), and dendrites were imaged in L1 of the barrel cortex during whisker stimulation trials. We confirmed these were tufted dendrites from putative pyramidal neurons based on 1) the presence of dendritic spines (inset images for D1 and D2), and 2) volume imaging with 3D dendritic reconstruction after the experiment (data not shown). Left: AIP in L1 depicts individual dendritic branches from L2/3 neurons. Right: inset images for two dendritic branches [D1 (top) and D2 (bottom)] and normalized $Ca^{2+}$ fluorescence traces for 11 whisker stimulation trials before (baseline) and with superfusion of DL-APV. Stim. = a single 40 ms whisker stimulation.

(**J – K**) A cocktail of inhibitors for GluRs inhibited neuropil $Ca^{2+}$ activity in L1 (combined L1a and L1b) during whisker stimulation trials in the same FHM2.Thy1GCaMP6s mice as

Figure 4H – J, demonstrating significant inhibition of GluR-mediated $Ca^{2+}$ activity in neurons. (J) An example of averaged traces from five whisker stimulation trials before (baseline; green) and with superfusion of GluR inhibitors (purple) from the same animal as Figure 4I. Stim. = 400 ms, 1 Hz, for 4 s. Responses averaged over the entire field of view under 2P. Spikes in the baseline trace (green) near the middle of the trace are due to movement artifact. (K) Quantification of the peak amplitude of neural $Ca^{2+}$ fluorescence during whisker stimulation trials for all mice (n = 5 FHM2.Thy1GCaMP6s mice).

B, D, E, K = paired samples *t*-test, one-tailed. Grey is animal mean, and color is grand mean. 'Box whisker' represents the median (horizontal line), IQR ('box'), 1.5*IQR ('whiskers'), and >1.5 times the IQR ('+'). Bar graphs represent the grand mean with the standard error of the mean. I = WT, while all other figure panels are from FHM2.

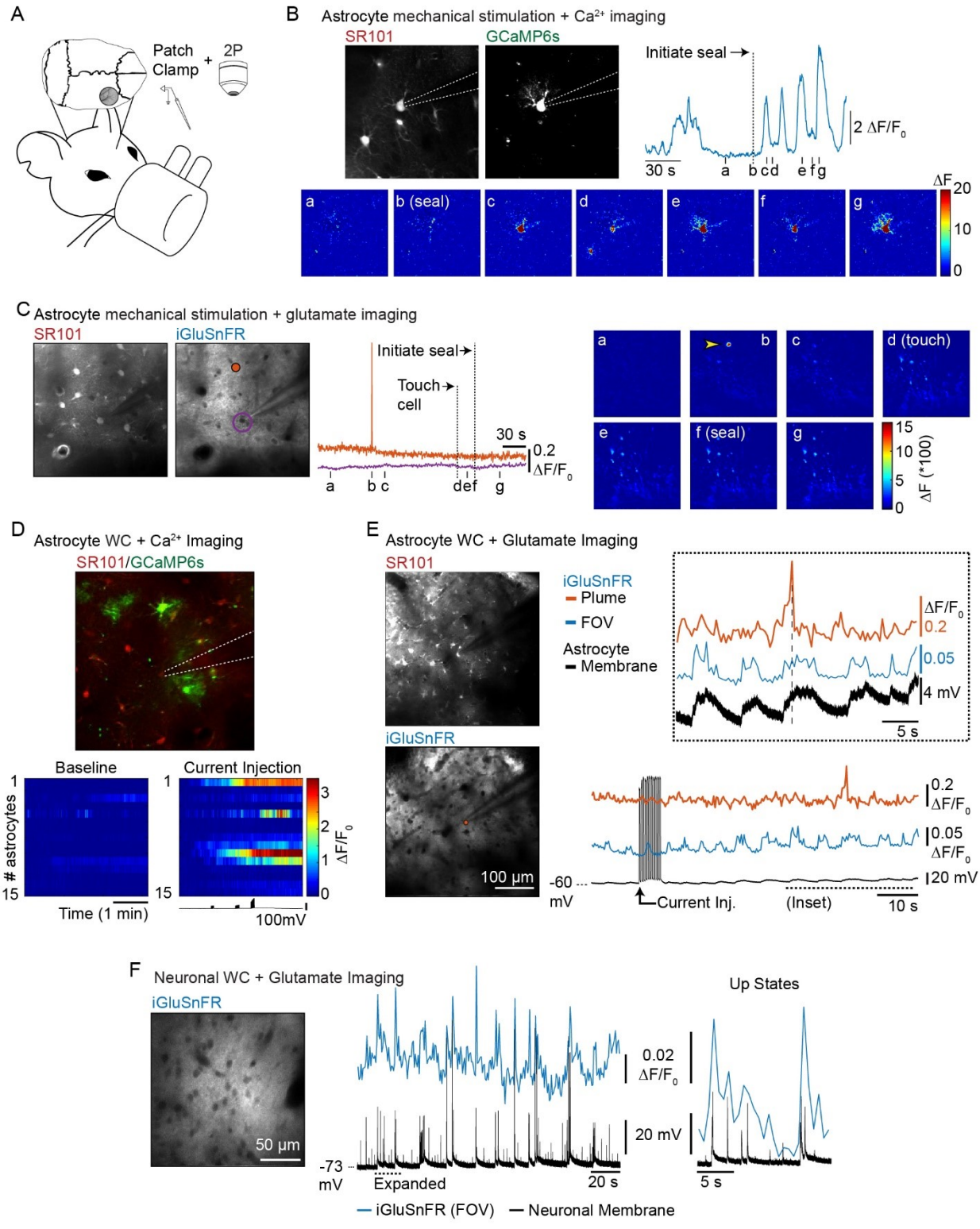
A
Patch Clamp + 2P
B
Astrocyte mechanical stimulation + Ca2+ imaging
SR101
GCaMP6s
Initiate seal
2 ΔF/F0
30 s
a b cd e f g
ΔF
20
10
0
a
b (seal)
c
d
e
f
g
C
Astrocyte mechanical stimulation + glutamate imaging
SR101
iGluSnFR
Initiate seal
Touch cell
30 s
0.2 ΔF/F0
a b c def g
a
b
c
d (touch)
e
f (seal)
g
15
10
5
0
ΔF (*100)
D
Astrocyte WC + Ca2+ Imaging
SR101/GCaMP6s
Baseline
Current Injection
# astrocytes
1
15
Time (1 min)
100mV
3
2
1
0
ΔF/F0
E
Astrocyte WC + Glutamate Imaging
SR101
iGluSnFR
Plume
FOV
Astrocyte
Membrane
ΔF/F0
0.2
0.05
4 mV
5 s
iGluSnFR
100 μm
0.2 ΔF/F0
0.05 ΔF/F0
-60 mV
20 mV
Current Inj.
(Inset)
10 s
F
Neuronal WC + Glutamate Imaging
iGluSnFR
50 μm
Up States
0.02 ΔF/F0
20 mV
-73 mV
Expanded
20 s
5 s
iGluSnFR (FOV)
Neuronal Membrane

**Figure S5: Astrocyte stimulation does not directly induce glutamatergic plumes (related to Figure 4).**

Astrocyte glutamate release that causes NMDA-mediated slow inward currents in neurons can occur spontaneously, and can be induced experimentally by increasing astrocyte $Ca^{2+}$ (Angulo et al., 2004; Fellin et al., 2004). It thus could be considered as a potential source of glutamate during plumes. However, *spontaneous* slow inward currents are reportedly $Ca^{2+}$-independent, and are unaffected by bafilomycin A1 (Gómez-Gonzalo et al., 2018; Perea and Araque, 2005) – these findings are in direct contrast with the mechanisms of release in spontaneous glutamatergic plumes.

Alternatively, mechanical stimulation of astrocytes is sufficient to induce $Ca^{2+}$-mediated glutamate release from astrocytes (Angulo et al., 2004; Araque et al., 1998a, 1998b, 2000; Innocenti et al., 2000; Ni and Parpura, 2009). Moreover, depolarizing a single astrocyte with current injections during whole-cell patch-clamp increases intracellular $Ca^{2+}$ in multiple astrocytes (Poskanzer and Yuste, 2011), providing an additional experimental means of inducing gliotransmission within a given region (Kang et al., 1998). Optogenetic depolarization of astrocytes is also linked to astrocyte glutamate release (Perea et al., 2014; Sasaki et al., 2012), further suggesting that astrocyte depolarization is also a sufficient means to study gliotransmission. We directly tested the potential of astrocyte glutamate release during plumes by directly manipulating astrocytes with the following experiments:

(**A**) Schematic of the experimental setup. We mechanically stimulated astrocytes *in vivo* by touching the cell soma and forming a seal with a patch pipette while simultaneously recording glutamate fluorescence with two-photon microscopy (2P) in superficial L1 in

anesthetized FHM2 mice (urethane or isoflurane). In addition, we used depolarizing current injections with whole-cell patch-clamp (current-clamp mode) with 2P glutamate imaging.

(**B**) Astrocyte mechanical stimulation increases intracellular $Ca^{2+}$ *in vivo*. We used SR101 to label astrocytes (Nimmerjahn and Helmchen, 2012) to guide a patch pipette in mice expressing the genetically encoded $Ca^{2+}$ indicator GCaMP6s in astrocytes under the Aldh1l1 promoter (see STAR Methods) (Srinivasan et al., 2016). Top left images = averaged intensity projections from a ~ 60 s period. Dashed lines outline the pipette. We confirmed that toughing and forming a seal on the soma of astrocytes induced a large $Ca^{2+}$ response in the cell body, as well as the fine processes distal from the soma (top right = example trace from a single cell; changes in fluorescence intensity averaged over the entire domain of the stimulated cell within the imaging plane; $Ca^{2+}$ response to touching the cell with the pipette are not shown). Bottom panels: select images from the same cell illustrate the increase in $Ca^{2+}$ fluorescence in the soma and processes of the astrocyte, as well as an adjacent astrocyte (panel d, lower left), after forming a seal with the pipette. Lowercase letters correspond with the time points in the above fluorescence trace.

(**C**) Astrocyte mechanical stimulation does not induce plumes *in vivo*. We used SR101 to guide astrocyte stimulation during fluorescent glutamate imaging (iGluSnFR). Left images are average intensity projections from a ~ 60 s period. A region of interest surrounding the stimulated astrocyte was collected to measure changes in glutamate fluorescence (including plumes) after touching and forming a seal on the cell (purple circle; quantification is the purple trace in the center). No plumes occurred in the field of view

during or > 60 s following astrocyte stimulation. An additional region of interest (orange) illustrates the location and size of a glutamatergic plume that occurred in the field of view prior to astrocyte stimulation (orange trace in the center; yellow arrowhead in the panels to the right). Right panels: select images taken from the same recording illustrate a glutamatergic plume (panel b) that occurred before stimulation, while no plume occurred after astrocyte stimulation. Note: punctate areas of increased fluorescence in panels c – g are due to translation of the tissue within the field of view over time and are not due to increases in glutamate fluorescence. Lowercase letters correspond with the time points in the fluorescence traces to the left. A representative of n = 9 astrocytes from 3 FHM2 mice.

(**D**) Depolarizing current injections in astrocytes increases intracellular $Ca^{2+}$ *in vivo*. Left: SR101 was used to guide *in vivo* astrocyte patch in mice expressing GCaMP6s under the Aldh1l1 promoter (See STAR Methods). The dashed line outlines the patch pipette. Average intensity projections taken from a ~ 60 s period. Bottom: Intensity raster plots quantify $Ca^{2+}$ fluorescence of the same 15 astrocytes within the field of view over time during baseline (whole-cell but no current injection) and with current injection. Membrane voltage of the patched astrocyte (the black trace in the lower right) is synchronized with the above raster plot to illustrate when a train of current injections occurred (500, 1,000, and 1,500 pA). A representative of n = 3 mice.

(**E**) Depolarizing current injections in astrocytes did not increase the frequency of glutamatergic plumes *in vivo*. Left: average intensity projections for SR101 and iGluSnFR, with a plume overlay (colored circle) illustrating the location and size of a plume that occurred near the patch pipette. WC = whole-cell. Right, bottom: iGluSnFR fluorescence

traces from the plume region of interest (top; orange) and the field of view (FOV; center, blue) are synchronized with the astrocyte membrane recording (black; bottom) to illustrate when the plume occurred relative to trains of depolarizing current injections. Top inset: An expanded view of the traces below. During whole-cell patch clamp, we found recurrent astrocyte membrane depolarizations (bottom black trace). Fluctuations in glial membrane potentials are closely correlated with fluctuation in neural membrane potentials, field potentials, and fluctuations in extracellular $K^+$, providing a measure of recurrent cortical network activity (Amzica, 2002; Mishima and Hirase, 2010). We confirmed a previous report that iGluSnFR fluorescence measured across the FOV (middle blue trace) oscillated (Xie et al., 2016) and correlated with the fluctuations in astrocyte membrane potential. Plumes predominantly occurred during the 'up' phase of the astrocyte membrane depolarization (top orange trace), with a probability of 0.833 across all animals (n = 3 mice). The vertical dashed line indicates the time of the peak of the plume. Alternatively, the probability that plumes occurred during astrocyte current injections (Current Inj.) was 0.22, suggesting plumes were more closely tied with cortical network activity than astrocyte membrane depolarization, per se [though astrocytes themselves likely influence cortical states (Poskanzer and Yuste, 2011, 2016)]. A representative of n = 5 astrocytes from 4 FHM2 mice.

(**F**) We confirmed that the oscillations in iGluSnFR fluorescence correlated with neuronal membrane fluctuations *in vivo*. Left: an average intensity projection of iGluSnFR fluorescence in L2/3 adjacent to a whole-cell patch-clamped neuron (putative pyramidal cell). Center: Synchronized iGluSnFR fluorescence and neuronal membrane potential. The recurrent depolarizations in the neuronal membrane are 'up states' under urethane

anesthesia, while the largest amplitude depolarizations are action potentials. Right: an expanded view of both traces.

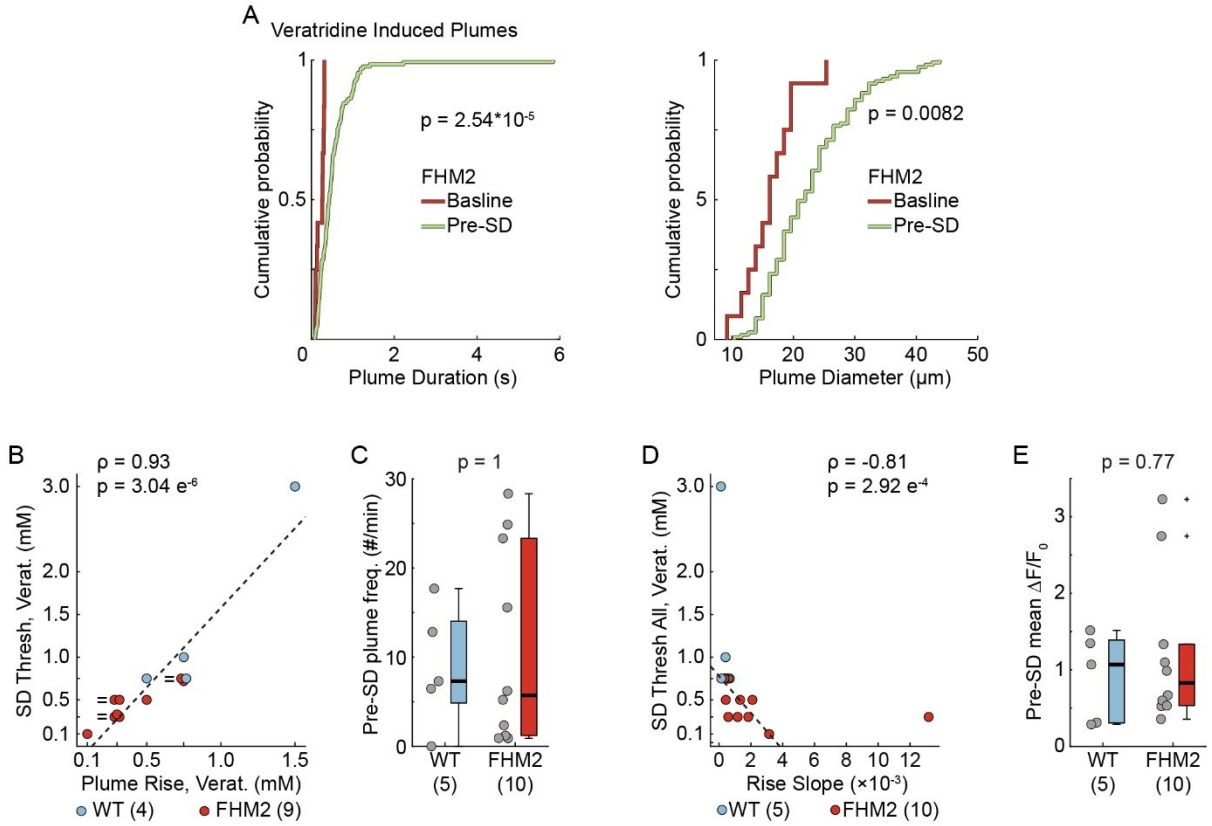
A
Veratridine Induced Plumes
Cumulative probability
p = 2.54*10-5
FHM2
Basline
Pre-SD
Plume Duration (s)
p = 0.0082
Plume Diameter (μm)
B
ρ = 0.93
p = 3.04 e-6
SD Thresh, Verat. (mM)
Plume Rise, Verat. (mM)
WT (4)
FHM2 (9)
C
p = 1
Pre-SD plume freq. (#/min)
WT (5)
FHM2 (10)
D
ρ = -0.81
p = 2.92 e-4
SD Thresh All, Verat. (mM)
Rise Slope (×10-3)
WT (5)
FHM2 (10)
E
p = 0.77
Pre-SD mean ΔF/F0
WT (5)
FHM2 (10)

**Figure S6. Extended data for glutamatergic plumes during veratridine induced SD (related to Figure 5).**

(**A**) Glutamatergic plumes that occurred just prior to veratridine induced SD (Pre-SD) were longer duration (left) and larger diameter (right) compared to plumes that occurred at baseline in FHM2 mice. Two-sample Kolmogorov-Smirnov test. n = 13 plumes (baseline) and 130 plumes (pre-SD) from the same 6 FHM2 mice as Figure 5D – L.

(**B – E**) To correlate the rise in plume frequency and basal glutamate fluorescence with SD onset, we performed an additional analysis expanding the number of FHM2 mice. We included WT and FHM2 mice from our original analysis (Figure 5D – L ), and added FHM2 control mice from our $Ni^{2+}$ experiments (control solution + veratridine) (Figure 5M – O).

(**B**) When it occurred, the rise in plume frequency correlated with SD threshold across individual animals, regardless of genotype. Note that several points overlapped on the graph, so they were offset for visualization and marked with '=' in the figure.

(**C**) The frequency of plumes prior to SD (at relative concentrations of veratridine for individual mice) was similar between WT and FHM2 mice.

(**D**) The slope of the rise in basal glutamate fluorescence correlated with SD onset (concentration of veratridine). The slope was measured as in Figure 5J. Fit used bisquare weighting.

(**E**) The level of basal glutamate fluorescence (mean $\Delta F/F_0$) at the concentration of veratridine that induced SD in individual mice was comparable in both genotypes.

n = # mice in parentheses. C, E = Wilcoxon rank-sum. B, D = Spearman's Rho. 'Box whisker' represents the median (horizontal line), IQR ('box'), 1.5*IQR ('whiskers'), and >1.5 times the IQR ('+'). Two mice were excluded from B (one from each genotype) because a rise in plume frequency did not occur. These mice were included in C – E.

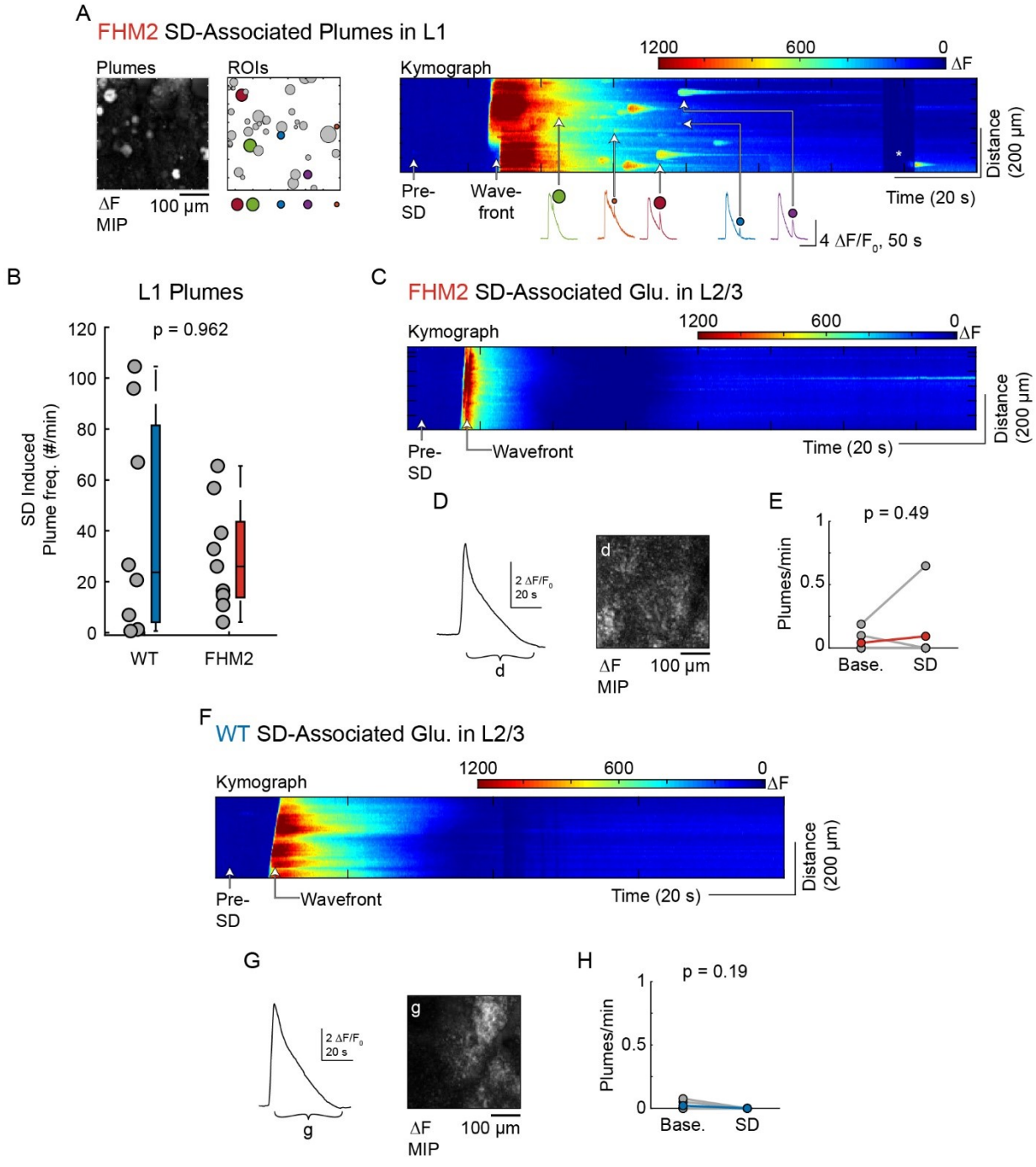
A
FHM2 SD-Associated Plumes in L1
Plumes
ROIs
ΔF MIP
100 μm
Kymograph
1200
600
0
ΔF
Distance (200 μm)
Pre-SD
Wave-front
Time (20 s)
4 ΔF/F0, 50 s
B
L1 Plumes
p = 0.962
SD Induced Plume freq. (#/min)
120
100
80
60
40
20
0
WT
FHM2
C
FHM2 SD-Associated Glu. in L2/3
Kymograph
1200
600
0
ΔF
Distance (200 μm)
Pre-SD
Wavefront
Time (20 s)
D
2 ΔF/F0
20 s
d
ΔF MIP
100 μm
E
p = 0.49
Plumes/min
1
0.5
0
Base.
SD
F
WT SD-Associated Glu. in L2/3
Kymograph
1200
600
0
ΔF
Distance (200 μm)
Pre-SD
Wavefront
Time (20 s)
G
2 ΔF/F0
20 s
g
ΔF MIP
100 μm
H
p = 0.19
Plumes/min
1
0.5
0
Base.
SD

**Figure S7. Extended data for plumes during the SD depolarization phase (related to Figure 7).**

(**A**) Similar to WT, plumes followed but did not precede the SD wavefront in L1 in FHM2 mice. Left: A MIP from the ΔF image series provides a spatial map of all plumes that occurred in the field of view during SD depolarization (following the wavefront). Center: A map of the ROIs for each plume (grey and colored circles). ROIs for a select set of plumes are colored and highlighted below the field of view and correspond with quantified events to the right. Right: A ∆F kymograph from the entire field of view illustrates the SD wavefront and all glutamatergic plumes over time. The presence of plumes during SD depolarization, without a significant increase in frequency prior to SD, is representative of all FHM2 mice imaged (n = 9 mice). The white arrows highlight a select set of plumes within the kymograph and correspond with the traces of glutamate fluorescence below. In all traces, the initial rise in fluorescence is the glutamate SD wavefront, while the colored ROI sits directly above the plume. It is possible that some plumes occurred with the propagating SD wavefront, but were indistinguishable from the high basal and rapidly changing glutamate fluorescence associated with SD. However, the amplitude of some plumes was similar to or even larger than the peak of the basal fluorescence during SD, suggesting the indicator (iGluSnFR) was not saturated by the SD wavefront and could still detect glutamate release associated with plumes. * = an imaging artifact due to the washout of the KCl.

(**B**) There was no difference in the frequency of plumes in L1 during SD depolarization in WT vs. FHM2 mice. Wilcoxon rank-sum. n = 8 WT and 9 FHM2 mice.

(**C – E**) Characterization of plumes during SD depolarization in L2/3 in FHM2 mice.

(**C**) A ∆F kymograph from the entire field of view during SD propagation in L2/3 from a FHM2 mouse. Note that no plumes occurred in this animal, representative of the general lack of plumes in L2/3 during SD in all mice recorded (n = 7 FHM2 mice). Glu. = glutamate.

(**D**) Left: Quantification of glutamate fluorescence during the same SD as in C. d = the phase of the glutamate wave corresponding to the ∆F MIP (Right). Note the lack of plumes in the MIP.

(**E**) The frequency of plumes during SD depolarization in L2/3 in FHM2 mice did not change relative to baseline recordings (prior to SD induction; n = 7 mice). Note: the y-axis is more than two orders of magnitude smaller than the y-axis for plume frequency in L1 during SD depolarization (Figures 7E and 7H). Note that 5 of the 7 mice had 0 plumes/min at baseline and during SD depolarization, and their data points are overlapping in the figure.

(**F – H**) Characterization of plumes during SD depolarization in L2/3 in WT mice.

(**F**) A ∆F kymograph from the entire field of view during SD propagation in L2/3 from a WT mouse. Note that no plumes occurred in this animal, representative of the general lack of plumes in L2/3 during SD in all mice recorded (n = 6 WT mice). Glu. = glutamate.

(**G**) Left: Quantification of glutamate fluorescence during the same SD as in F. g = the phase of the glutamate wave corresponding to the ∆F MIP (Right). Note the lack of plumes in the MIP.

(**H**) The frequency of plumes during SD depolarization in L2/3 in WT mice did not change relative to baseline recordings (prior to SD induction; n = 6 mice). Note: the y-axis is more than two orders of magnitude smaller than the y-axis for plume frequency in L1 during SD depolarization (Figures 7E and 7H).

A, C – E = FHM2. F – H = WT. E and H = paired-samples t-test.